Sea Surface Scattering under Rainy Conditions

David Lemaire and Piotr Sobieski

UCL Belgium

1 Introduction

Under the topic "surface scattering" in the EuroTRMM project (1) we developed a method to combine the wind wave spectrum with the spectrum of rain-generated waves, (2) we provided an electromagnetic backscattering model for the simulation of ocean surface echoes in the PR configuration and (3) we provided a model of the ocean surface emissivity for the simulation and the inversion of the TMI measurements. Moreover (4) we performed a comparison between two electromagnetic models of the scattering by rough surfaces, i.e. the Boundary Perturbation Method (BPM) that we had developed in the framework of previous ESA studies and the Integral Equation Method (IEM) known from the literature; and (5) we used the synergy between active and passive microwave observations in an inversion procedure to retrieve the surface wind speed, the integrated water vapor and liquid water contents from co-located TMI and PR measurements.

2 The *UCL* physical model

2.1 The sea surface model

As wind is blowing over the ocean, it generates tangential stresses over the water surface. Due to these friction stresses, gravity-capillary waves quickly appear on the surface. The energy of these waves is related to the intensity of the friction stresses. As wind continues to blow, the wind energy entering through small gravity-capillary waves is partly transmitted to longer gravity waves through non-linear wave-wave interactions, and partly dissipated. Then, as time elapses, the wave energy, initially associated with small waves, grows and is transferred to waves with longer and longer wavelength. The process continues until an equilibrium is reached between energy input from the wind and energy dissipation by wave breaking, turbulence and viscosity.

The problem of the air-sea interaction has been discussed here by concentrating in a first step on the gravity range, the intermediate gravity-capillary range and the capillary range of the wind wave spectrum. The angular spreading function has been considered either. One originality is that in our model, the large gravity waves are characterized geometrically, i.e. independently of their generating mechanisms and thus of environmental parameters such as the wind. The formulation is based on field experiments. The gravity-capillary waves strongly influence the radar scattering. Until now the gravity-capillary wave spectrum was derived from measured temporal spectra. Very recently several authors have presented direct wavenumber spectra measured in wavetanks or in natural conditions. The gravity-capillary part of the wind wave spectrum in the UCL model is based on those recent measurements. For the capillary domain, the UCL model implements the classical Cox viscous cutoff spectrum. In this section the gravity, gravity-capillary and capillary spectra discussed above are combined. The full range spectrum is finally constructed as an slightly non-linear combination of each component.

Beside wind a rain induced ringwave spectrum has been taken into account also. It is based on frequency spectra of the surface elevation measured for monodisperse rain with 2.8mm drops and for various rain rates at the NASA Wallops Flight Facility. More recent measurements of the ringwave spectrum were also

performed in the case of monodisperse rain with other drop sizes and in the case of polydisperse rain but the results of these experiments were not available on time for this study.

The combined wind and rain wave surface elevation spectrum is rather different from their simple sum. In particular, the damping of sea waves by rain is often reported. Indeed, as drops hit and enter the water surface, they generate vortices and turbulence in the upper water layer close to the surface. As a result, the turbulent viscosity is increased which in turn affects the generation of wind and ring waves. To evaluate the spectrum combination, we established equilibrium relationships between the energy input from wind and rain as well, and the output from viscosity and other dissipation sources. With a number of well identified hypotheses, we identified the different input and output contributions in the case of combined wind and rain conditions, which then lead to the determination of an equilibrium spectrum.

The model developed following this approach has already been analyzed in depth in previous studies. Two important results should be underlined. For high wavenumbers, the equilibrium spectrum is an intermediate solution between the sum spectrum and the maximum of the wind and the rain spectra. For lower wavenumbers, the combined spectrum can be lower than the wind only spectrum, especially at high rain rates and low wind speeds. This effect is of the order of a few dB (1 to 4 dB in extreme conditions) and is limited to a wavenumber band of about one decade.

The surface spectrum does not give a complete statistical definition of the surface roughness. Additional information is provided by the probability density function of the surface slope. The surface slopes largely affect the radar signals, and their influence on the NRCS can be expressed through their PDF. In our model we use a surface slope PDF as expressed by Cox and Munk's with Graham-Charlier expansion but corrected in several ways: (i) to account for the asymmetry of the surface slope with respect to the wind direction, (ii) to avoid the slope PDF becomes negative in the upwind direction, which is mathematically incorrect and (iii) with a scaling so that the PDF is coherent with slope variances computed from the spectrum.

To be complete the presence of foam is also taken into account but it will be used for radiometric measurements only.

2.2 The rough sea surface scattering model

The ocean surface is composed of many scales of roughness. Physical Optics and Bragg solutions apply strictly to *mm* waves and HF waves respectively. The IEM introduced by A.Fung takes the form of an series expansion and can yield a better solution over a larger range of wavelengths when enough terms of the expansion are used, but however becomes practically inapplicable when too many terms must be computed. In this study we present and compare two methods for the computation of the scattering by a composite surface. One is based on the BPM developed in our previous studies; the other is a two-scale extension of the IEM.

In the BPM, it is assumed that the surface is composed as the superposition of small ripples with *rms* values far much smaller than the EM wavelength, on large waves. The two surface components are assumed to be independent stochastic processes and their corresponding spectrum is computed by splitting the spectrum of the composite surface at a given wavenumber. This separating value has been analysed in this study. The total scattering coefficient is then expressed as the sum of two terms :

$$\sigma^o_{pq} = \sigma^o_{pq0} + \sigma^o_{pq1} \tag{2.1}$$

The zero order term is given by the Kirchhoff solution for the large scale surface with the Fresnel coefficient corrected to account for the effect of the ripples present on the large waves. The first order term results from the Fourier components of the surface spectrum that produce a constructive (Bragg) interference in the

scattering direction but from ripples lying on large tilting undulations, hence with a certain slope probability density, a certain range of Fourier components may have the correct wavelength and orientation to yield a constructive interference.

The other approach is based on a two-scale expansion of the IEM in which the surface fields appear as the sum of a Kirchhoff and a complementary term. The scattering coefficient appears as the sum of several terms:

$$\sigma^o_{pq} = \sigma^o_{pq0} + \sum_{n=1}^{\infty} \sigma^o_{pqn} + \sum_{m=1}^{\infty}\sum_{n=1}^{\infty} \sigma^o_{pqmn} \tag{2.2}$$

As with the BPM, the zero order term is given by Kirchhoff's solution for the large scale surface with an effective Fresnel coefficient taking into account the effect of the ripples with a correction w.r.t the BPM. The single scattering terms are given by a convolution between the ripples spectral functions and the large scale slope probability density function. This can be physically interpreted as resulting from the interaction between small waves propagating on large tilting waves. The higher order terms σ^o_{pqmn} take multiple scattering into account. They represent the influence of the electromagnetic fields at one point of the surface on the neighbouring points. They will not be considered in the following analysis.

Simulations have been performed for the ocean surface using the BPM and the two-scale IEM. We considered a large range of incidence angles for 3 different frequencies (5.3GHz, 13.6 GHz and 36GHz) and 3 incident-scattered polarization combinations (VV, HH, VH). We used the surface spectrum presented above with different wind friction velocities for a view angle aligned with the wind direction.

In most configurations, the difference between the BPM and the two-scale IEM results is small, if not negligible, w.r.t. the accuracy of radar measurements. The largest differences occur at large incidence angle, large wind (i.e. important roughness) and high frequency, where it is of the order of 1 dB. The difference is also slightly larger in HH than in the other polarization configurations. Considering the accuracy of usual remote sensing measurements and under the assumptions made for the models development, both methods give very similar results. Since the BPM is based on a simple physical argument and appears more efficient than the two-scale IEM w.r.t. computation time, the BPM should be preferred for ocean-like rough surfaces.

Figure 1 presents an example of results in VV polarization at 36 GHz and large wind friction velocity, i.e. for the configurations where the difference between the BPM and the two-scale IEM is the largest.

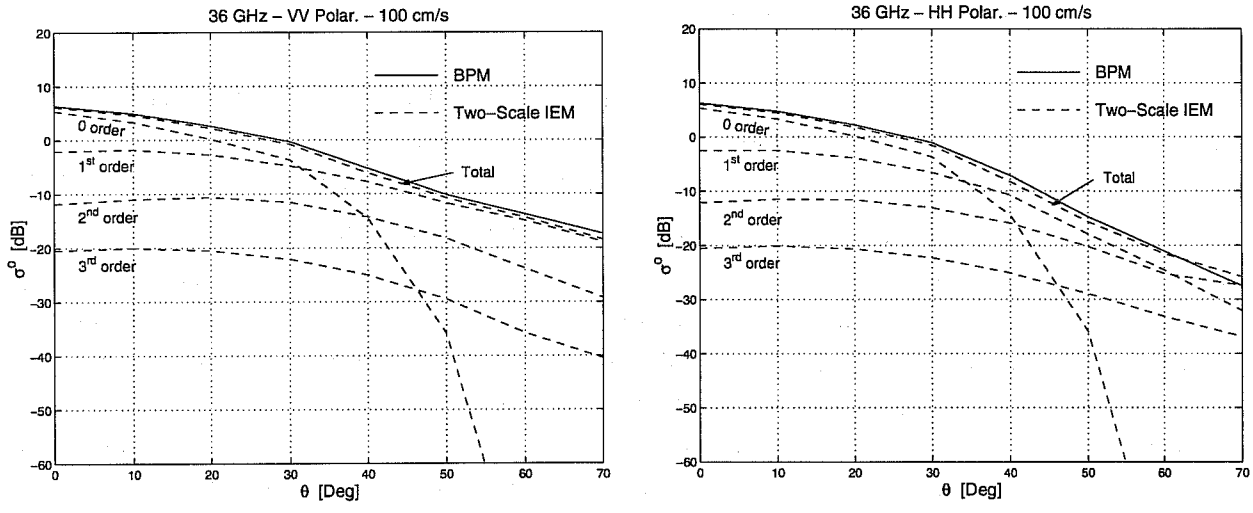

Fig 1: Successive terms of σ^o using the two-scale IEM (36 GHz, Left=VV, Right=HH.) and comparison with the BPM.

2.3 Sea foam

Several combinations of foam coverage models and foam emissivity models have been implemented during a previous joined study between UCL and CETP(F). Based on these, we have selected the model by Monahan and Lu for the foam coverage and Droppelman's model for the foam emissivity. Monahan and Lu model gives the foam coverage as a function of the 10-meter surface wind speed and seawater viscosity. The foam contribution to surface scattering is expressed by separating the sea surface into foam-free and foam-covered parts, proportionally to the foam coverage. The covered part is assumed with a uniform distribution of foam.

2.4 The atmosphere

The atmosphere is assumed stratiform and scatterer-free. The first assumption use horizontally homogeneous vertical profiles of the atmospheric constituents that have a significant impact on microwave propagation. This assumption simplifies extremely the implementation of the model. Obviously, it will be in default in the case of well localized clouds for instance as treated by other EuroTRMM partners. In clear sky conditions, the second assumption is valid in the microwave range. In rainy regions, the scattering by rain drops can be neglected at low frequency, but may become important as frequency increases. This effect is not considered in the UCL model.

3 Applications

3.1 Emissivity model

The emissivity in direction $\vec{s}$ and polarization q is the complement to unity of the "integrated reflectivity" and is given by :

$$e_q(\vec{s}) = 1 - \Gamma_q(-\vec{s}) \tag{3.1}$$

$\Gamma_P(\vec{i})$ is the fraction of the energy incident from direction $\vec{i}$ with polarization $\vec{p}$ (V or H), scattered into all directions of the hemisphere above the surface. It is given by :

$$\Gamma_p(\vec{i}) = \frac{1}{4\pi \cos\theta_i} \iint \left[\sigma^o_{pV}(\vec{s},\vec{i}) + \sigma^o_{pH}(\vec{s},\vec{i})\right] d\Omega_s \tag{3.2}$$

where $d\Omega_s$ is an elementary solid angle in direction $\vec{s}$.

The computation of the sea surface emissivity is much slower than for σ^o NRCS since the bi-static scattering coefficients must be evaluated for a large number of incident directions given TRMM observation angles, before integrating them to get the emissivity. Therefore, we computed first bi-static scattering coefficient matrices $\sigma^o_{pq}(\theta_i,\phi_i)$ as a function of the wind speed, wind direction, seawater temperature and rain rate, for the 9 channels of TMI. Then, we integrated these matrices through (3.2) to get the emissivity. For each polarization of TMI, we interpolated the results to get a single formula for the surface emissivity as a function of the frequency, wind speed, wind direction, seawater temperature and rain rate. Fortran and Matlab routines implementing the interpolation formula were made available. For a sea surface temperature of 300°K, the contribution of the interpolation errors to the standard deviation of modeled brightness temperatures, will be smaller than about 0.2°K if no atmospheric effect is considered. Figures 2 give examples of the computed emissivity, as a function various parameters included in our physical model.

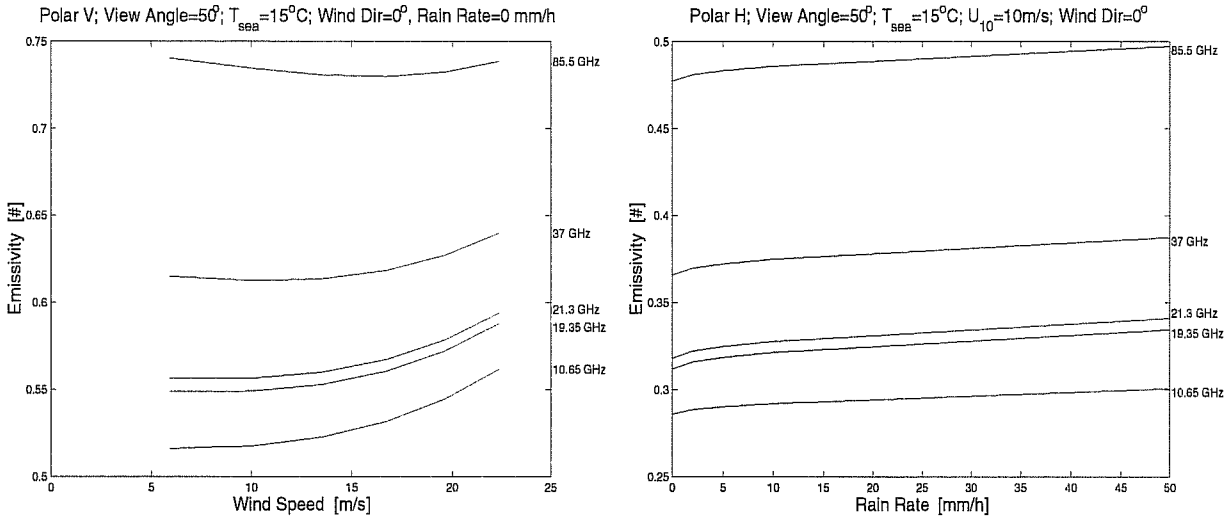

Fig. 2: Examples of ocean surface emissivity vs. wind speed and the rain rate.

3.2 Validation of PR and TMI simulations

3.2.1 Data

The data used to validate the UCL model consisted in the level 2A.21 version 4 PR surface normalized cross-sections and the level 1B.11 version 4 TMI brightness temperatures for TRMM orbit #4283 (containing Bonnie hurricane data). TMI data have furthermore been recalibrated using the algorithm later implemented in version 5 of TRMM products. The surface and atmosphere information was provided by co-located ECMWF analysis. The co-location criterion means a maximum distance of 50km with a time offset smaller than half an hour.

3.2.2 Results

Validation examples of TMI brightness temperatures and PR surface cross-sections are displayed on figures 3 and 4. For the PR, we observe a good agreement between the measurements and the simulations at low incidence angle (below 12 degrees), while the discrepancy between the computations and the data increases as the radar view angle largely departs from nadir. The quality of two-scale electromagnetic scattering models is worst in the range of incidence angle between 10 and 20 degrees, which is likely to be one reason of divergence between measurements and simulations above 12 degrees approximately. For TMI data, points with an integrated liquid content larger than 0.2 mm are not taken into account in the figures. We observe a fair agreement in the mean, with slopes of linear regressions between data and simulations close to unity, but however with large biases on some channels. There might be several reasons to explain these biases. First one might suspect the calibration error of the instrument, but the data were reprocessed using the very last version of the calibration procedure developed for the version 5 products. Next the scattering plus radiative transfer model might be suspected, but the same model previously used for the simulation of various radiometric sensors (TOPEX/TMR, ERS-1&2/ATSR, SSM/I) provided very good results.

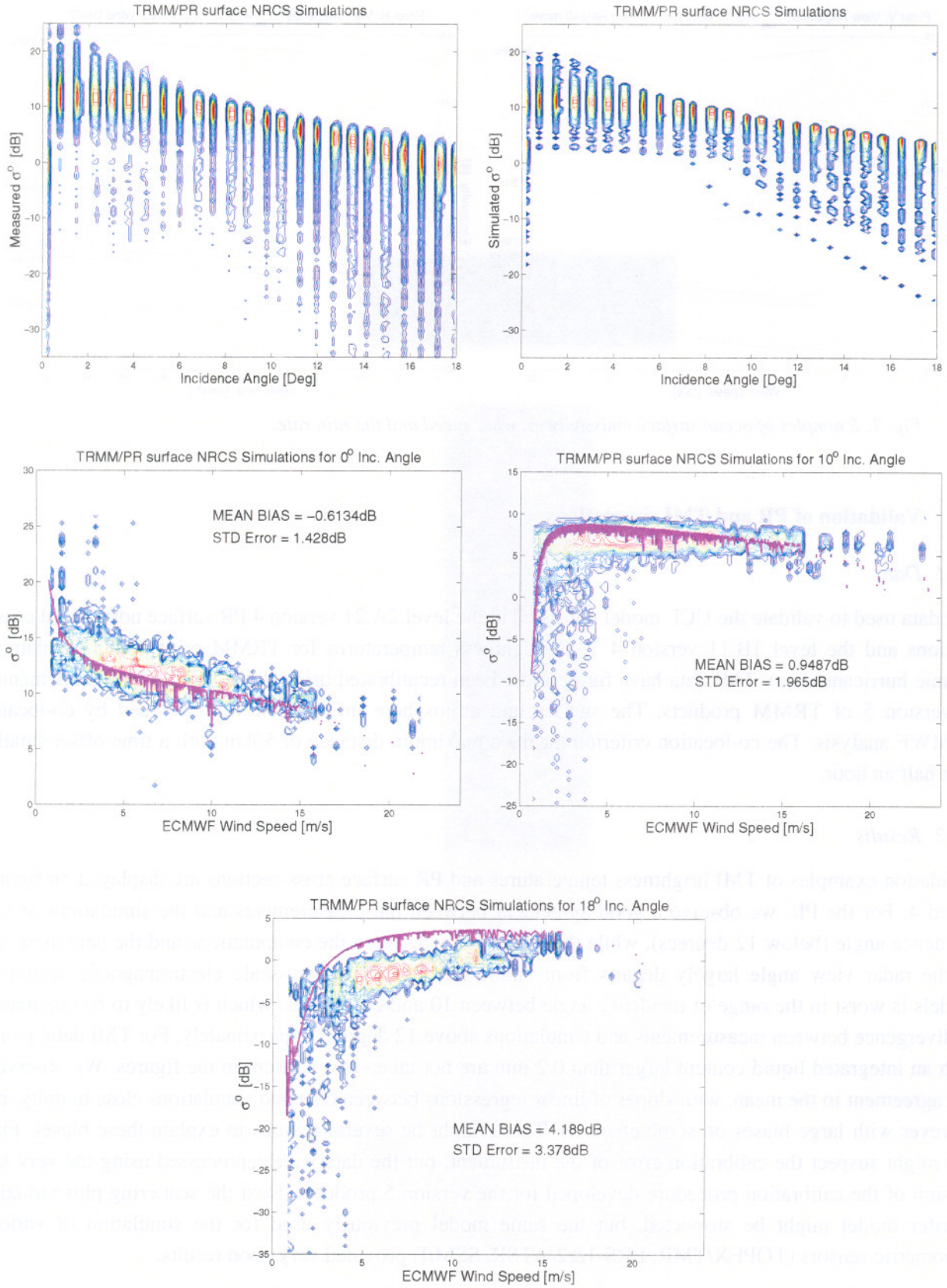

Fig. 3: PR surface cross-sections: simulations and measurements.

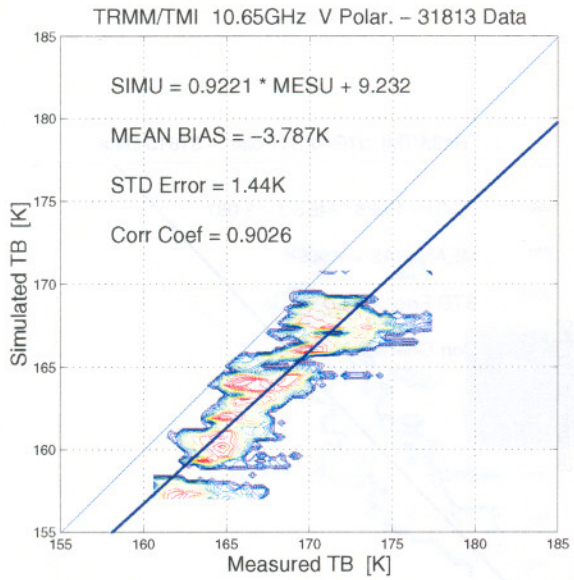
TRMM/TMI 10.65GHz V Polar. – 31813 Data
SIMU = 0.9221 * MESU + 9.232
MEAN BIAS = –3.787K
STD Error = 1.44K
Corr Coef = 0.9026
Simulated TB [K]
Measured TB [K]

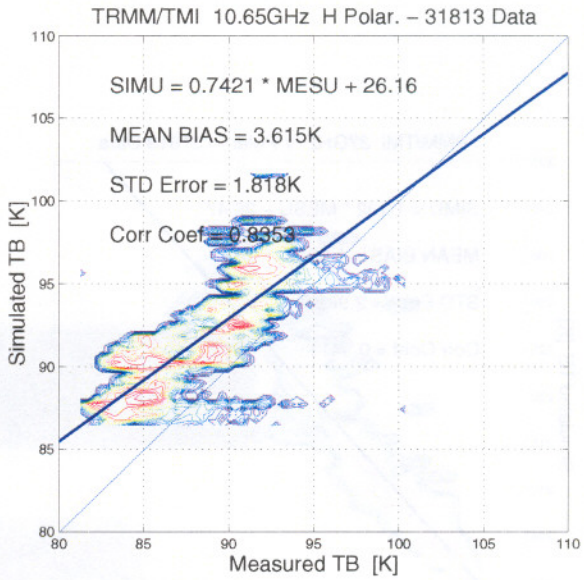
TRMM/TMI 10.65GHz H Polar. – 31813 Data
SIMU = 0.7421 * MESU + 26.16
MEAN BIAS = 3.615K
STD Error = 1.818K
Corr Coef = 0.8353
Simulated TB [K]
Measured TB [K]

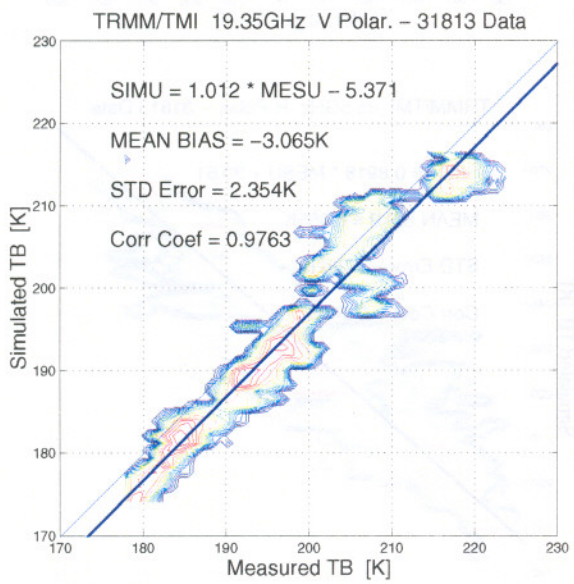
TRMM/TMI 19.35GHz V Polar. – 31813 Data
SIMU = 1.012 * MESU – 5.371
MEAN BIAS = –3.065K
STD Error = 2.354K
Corr Coef = 0.9763
Simulated TB [K]
Measured TB [K]

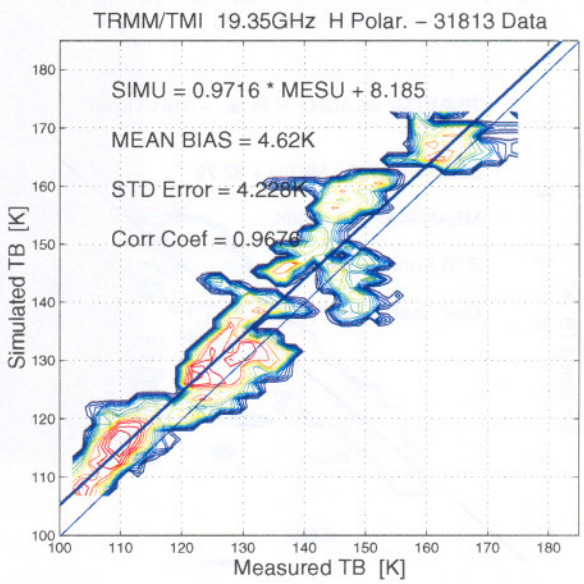
TRMM/TMI 19.35GHz H Polar. – 31813 Data
SIMU = 0.9716 * MESU + 8.185
MEAN BIAS = 4.62K
STD Error = 4.228K
Corr Coef = 0.9676
Simulated TB [K]
Measured TB [K]

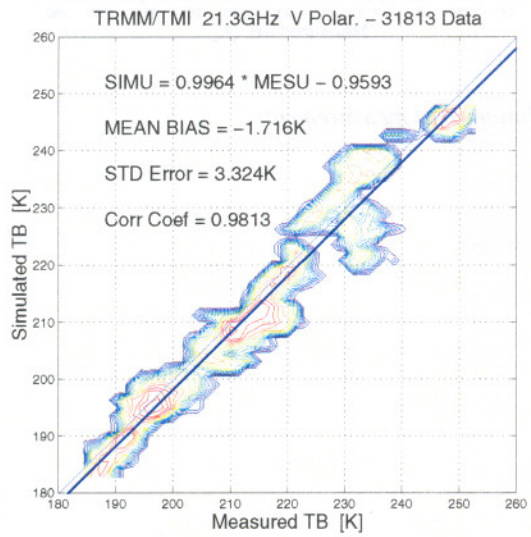
TRMM/TMI 21.3GHz V Polar. – 31813 Data
SIMU = 0.9964 * MESU – 0.9593
MEAN BIAS = –1.716K
STD Error = 3.324K
Corr Coef = 0.9813
Simulated TB [K]
Measured TB [K]

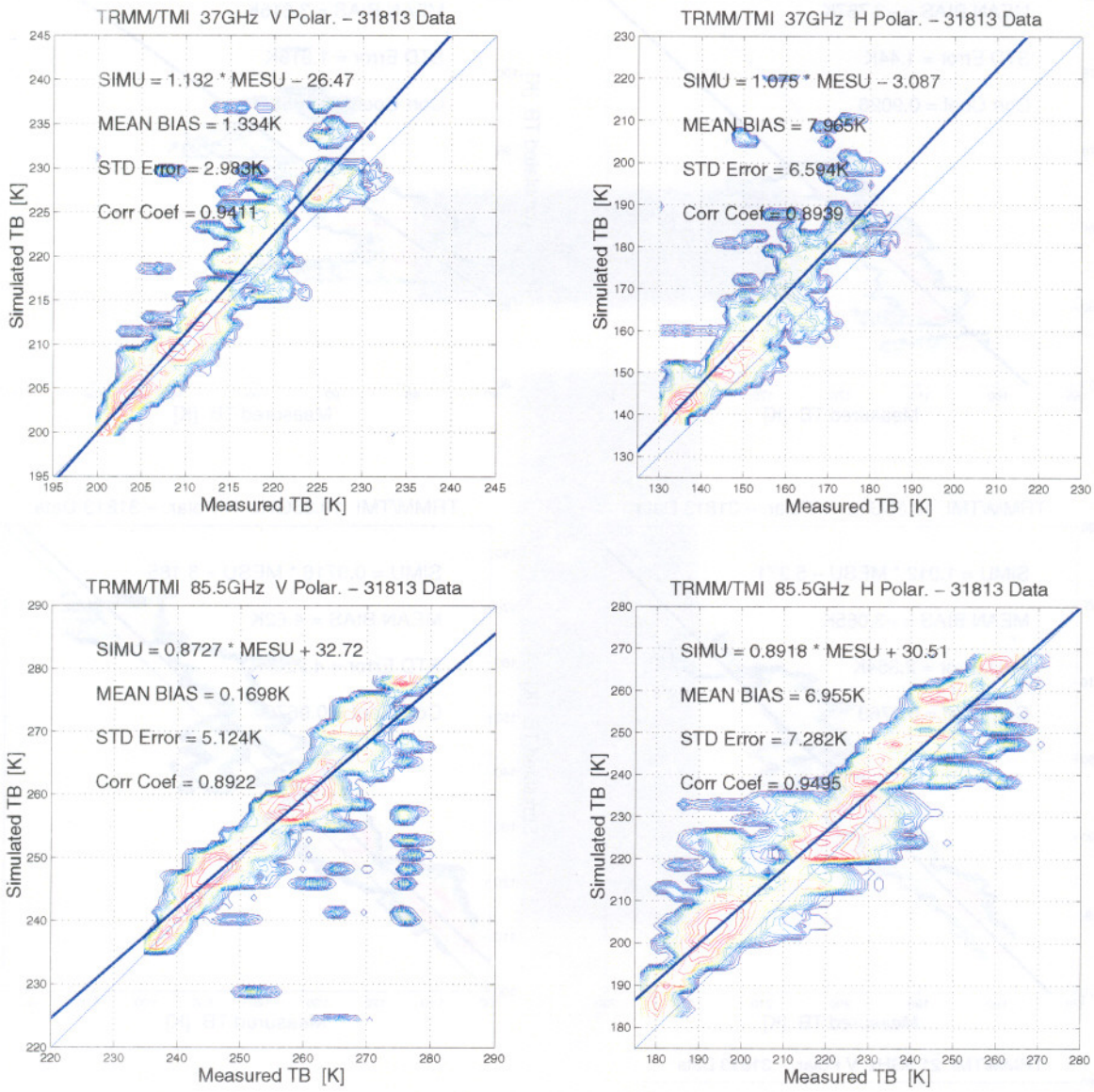

Fig. 4: TMI brightness temperatures: simulations and measurements.

3.3 Synergic inversion of PR and TMI measurements

The last part of this study consisted in a synergic inversion of TRMM TMI and PR co-located data for the retrieval of surface and atmosphere parameters. For those, we distinguish two cases : first we show the retrievals obtained using TMI only then using both TMI and PR in order to evaluate the benefit obtained from the synergy between active and passive measurements.

3.3.1 Two-step synergic inversion method

A large number of parameters have to be retrieved, describing either the sea state or the atmospheric conditions, hence we oriented the developments towards a two-step method to determine separately surface and atmosphere parameters. The idea is based on the observation that brightness temperature measurements in two polarizations at the same frequency can provide surface information with reduced sensitivity to atmosphere parameters. Having obtained a first approximation of the surface parameters, radiometric data can in turn be used to retrieve atmospheric parameters, that are further used to refine the estimation of surface retrievals, etc ... The method starts with a first rough a priori estimate of atmospheric parameters, that can be obtained from the adjacent ground cell. The complete inversion scheme is not presented here.

3.3.2 Data

The data used are those cited above for TRMM orbit #4283. We used however only a subset of these data corresponding to the Bonnie hurricane area. For the evaluation of the outputs, as for the simulations we used as ground truth, the data provided by ECMWF. The co-location criteria between TRMM and ECMWF data sets were as previously a maximum distance of 50km with a time offset smaller than half an hour while the co-location criteria required for TMI and PR data were a maximum distance of 15km. Note that the time offset remains always of the order of a minute due to the satellite instrumental configuration and flight scheme.

As only integrated contents are retrieved for the atmospheric parameters, profiles have to be fed into the inversion algorithm for the temperature, the pressure (to evaluate the absorption by dry gases), the water vapor and the liquid content. The information for these profiles is an a priori knowledge that may come from various sources : general approximate profiles for the atmosphere, average profiles observed in a given region under given conditions, information from meteorological models or more precise data from field campaigns. In this study we considered two cases. In a first situation, we considered theoretical profiles with a bilinear temperature dependence and exponential profiles for pressure and water vapor content. For clouds, a profile with constant liquid water content is taken between 5 and 6.5 km. In a second situation, we considered standard 31-level profiles provide by ECMWF forecasts at co-located areas. For the temperature and the pressure, we used the profiles themselves, while for the water vapor and the liquid water, we only used the shape of ECMWF profiles since their amplitude is determined by the integrated contents to be retrieved.

3.3.3 Inversion of TMI measurements

Figure 5 shows the results obtained when only TMI data are used in the inversion procedure. Out of the 80000 data points initially considered, only 35% are taken into account in the figure. Indeed, for the 65% remaining, a simple test indicates that the inversion procedure had not converged. Actually, it appears difficult to discriminate the influence of the seawater temperature on the surface signature from the influence of the surface wind speed, and oscillations between extreme values frequently occur. We also observe that the seawater temperature is very often retrieved at 30°C while the average seawater temperature provided by the ECMWF forecasts is 28°C. Therefore, in order to avoid the convergence problems, we proceeded to the

inversion of the same data set, with the seawater temperature fixed at 28°C. The results are presented in figure 5.The inversion converges in appreciatively 94% of the cases and, compared to ECMWF forecasts, there is less dispersion of the wind, while the correspondence (the angular coefficient of the linear regression) between the retrieved and the ECMWF values decreases. There is no major modification of the statistical characteristics of the integrated water vapor and liquid water retrievals.

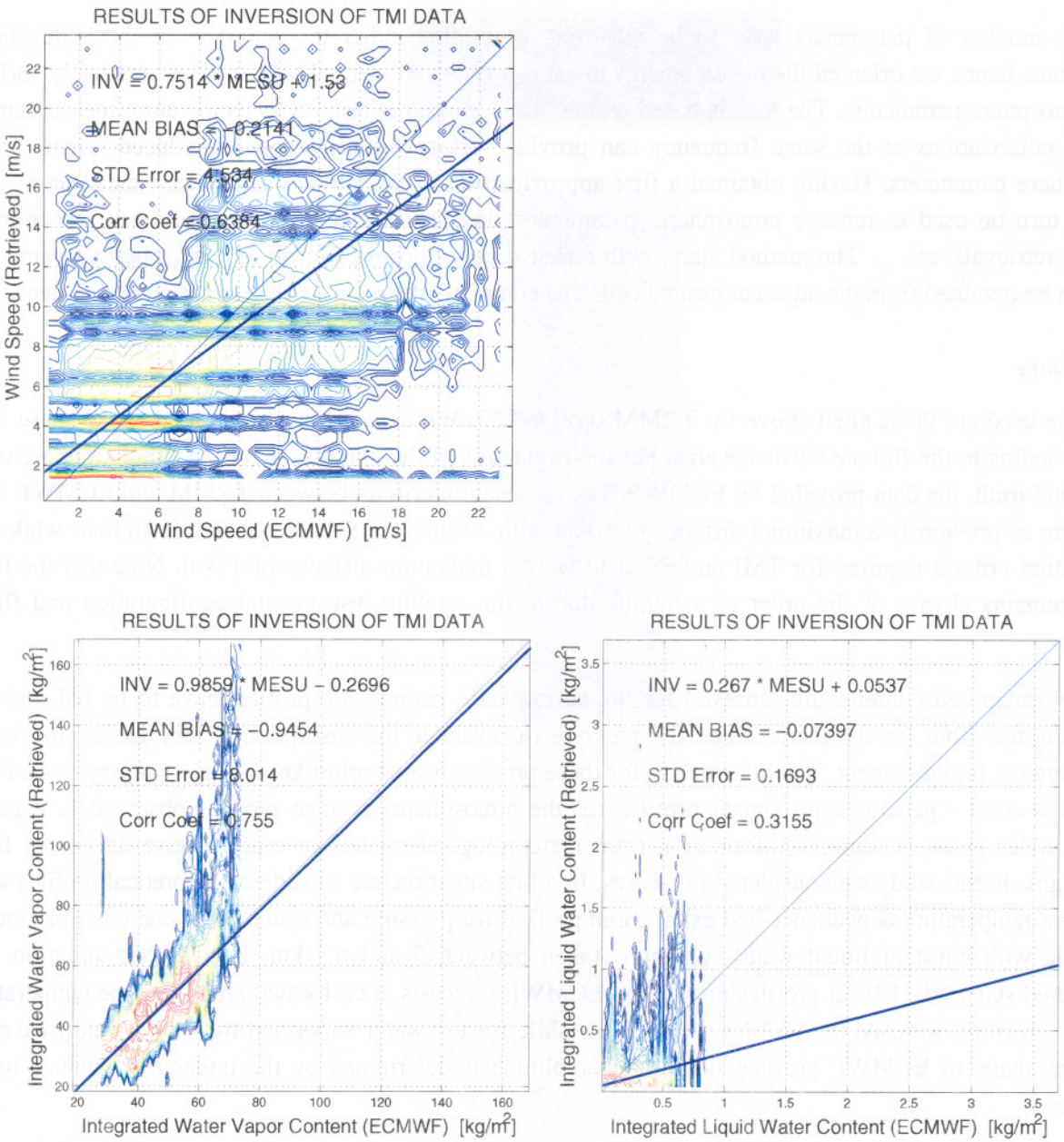

Fig. 5: Inversion results using the TMI measurements alone with fixed seawater temperature at 28°C.

3.3.4 *Inversion of co-located TMI and PR measurements*

In order to improve the results obtained in the case of TMI data only, we attempted to take profit from the synergy between active and passive instruments by including PR surface cross-section measurements into the inversion loop. The PR radar is sensitive to the surface roughness and less to the atmospheric constituents and to the water temperature. Thus, the PR data give more weight on the wind friction velocity in the inversion procedure, which in turn should first yield less ambiguity between the seawater and wind speed retrievals, i.e. it should improve the convergence of the method; and secondly, by improving the results for surface parameters, including PR data should also improve the atmospheric parameters retrievals.

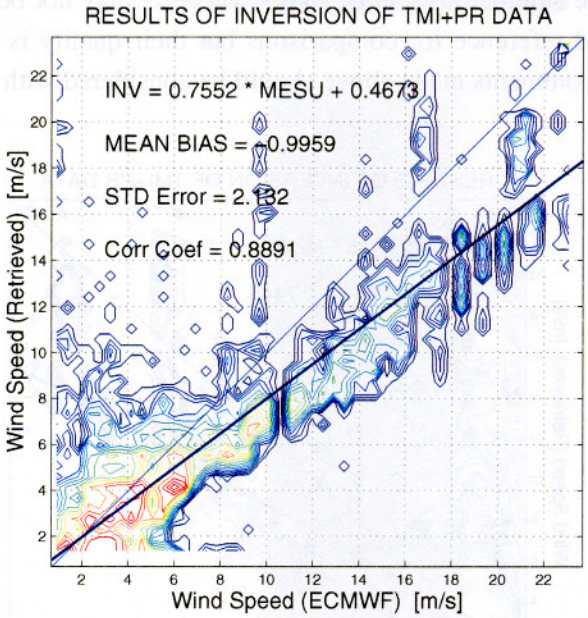

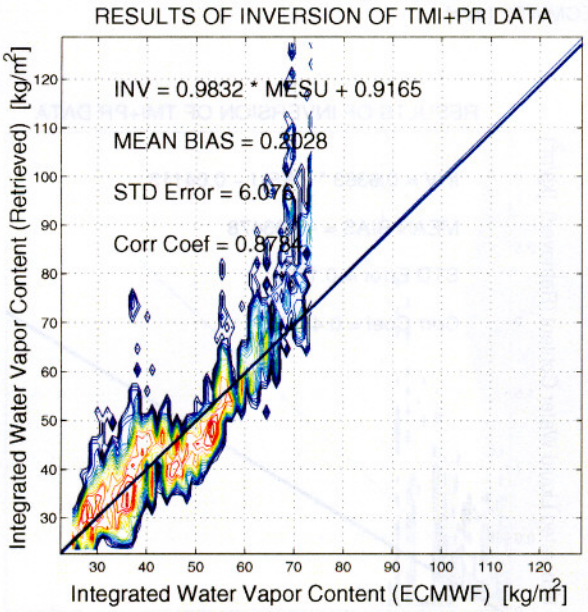

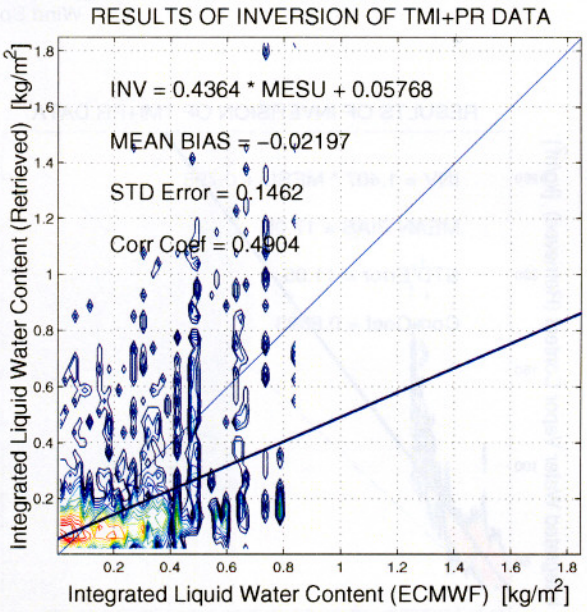

Fig. 6: Inversion results using synergy between TMI radiometric data and PR cross-section measurements, and assuming theoretical atmospheric profiles.

We considered first the case of theoretical atmospheric profiles to proceed to the inversion. The results are displayed on figure 6. As expected, the convergence rate is improved and reaches about 85% (Note however that due to the instrumental configuration aboard of TRMM, only 1/8 of the TMI data can be co-located with PR measurements). Next, for what concerns the quality of the retrievals, we note that, when compared with ECMWF forecasts, the wind speed and the water vapor contents are rather satisfactorily retrieved, while as before the seawater temperature is almost always retrieved at 30°C and the liquid water content compares poorly to ECMWF forecasts. For the seawater temperature, 30°C corresponds the upper limit considered in our inversion scheme and is also close to what is commonly observed in tropical regions. Therefore it is not easy to distinguish whether this value is retrieved due to divergence of the inversion algorithm or if it would be also retrieved with an enlarged temperature range considered in the inversion scheme. Note also that as mentioned in section 3.2 for the simulations, the ECMWF forecasts may not be considered as ground truth. They are assumed to be a good reference for comparisons but their quality is not precisely known for the tropical regions, so that all the comments made above should be considered with care.

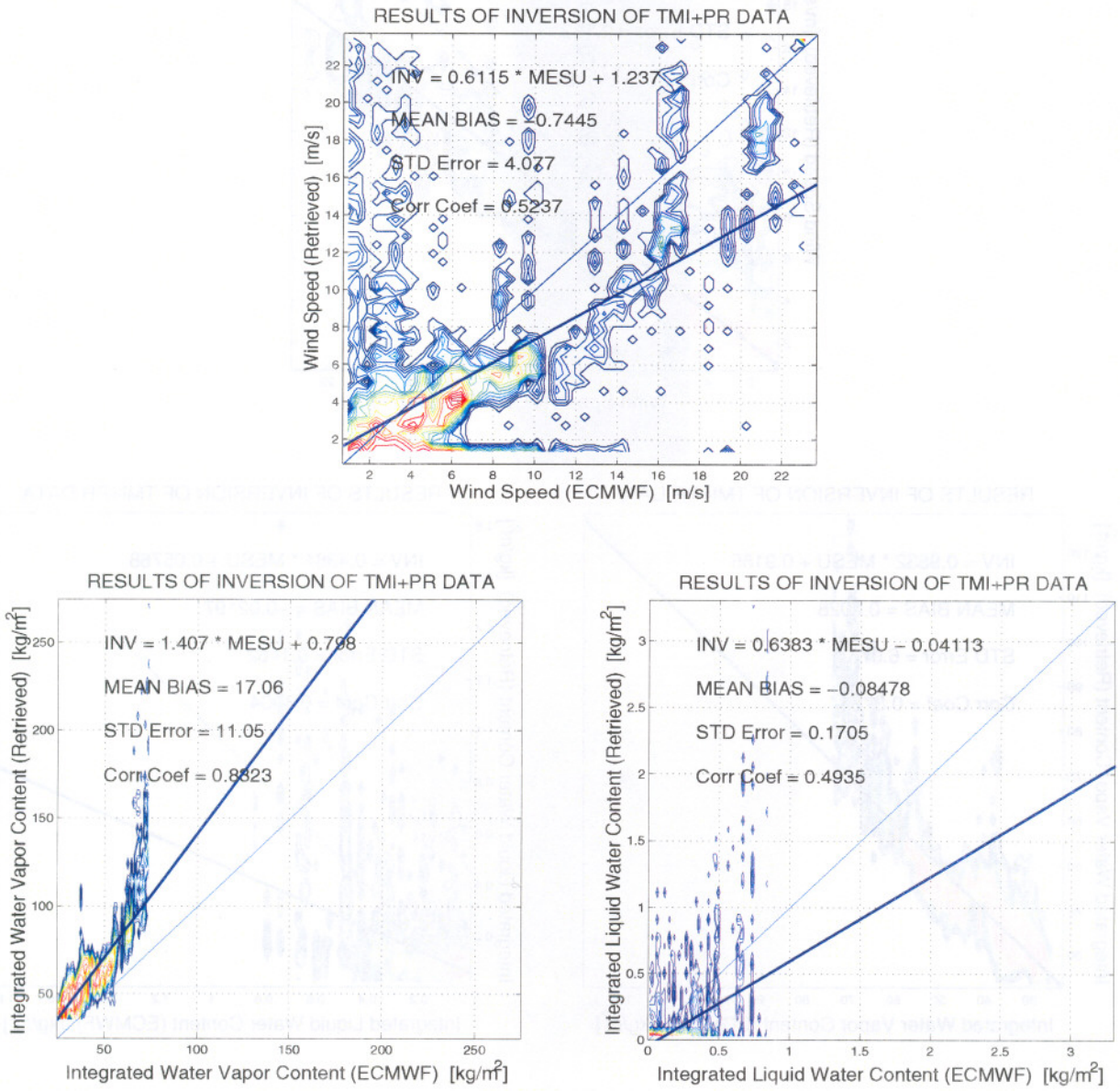

Fig. 7: Inversion results using synergy between TMI radiometric data and PR cross-section measurements, and ECMWF atmospheric profiles.

In a second situation, we used the ECMWF atmospheric profiles in the inversion procedure. The temperature and pressure profiles were used as given by the forecasts, while only the shape of the water vapor and liquid water profiles was taken into account. The results are displayed on figure 7, where we note a poor correspondence with ECMWF forecasts for all parameters. This may indicate that some of the parameters given in the forecasts do not correspond very well to the scene sensed by TRMM instruments. Among all parameters fixed in the inversion by using ECMWF profiles, the liquid water profiles - in conjunction with the temperature profiles that provide the cloud temperature - are the most likely to have the biggest impact on the retrieval. Again, as in the case of direct simulations of the measurements, we conclude that a comparison with campaign data would greatly help in the evaluation of the efficiency of the inversion method proposed, since it would help to discriminate between model- and method-related weaknesses and the quality of the data sets used.

4 CONCLUSIONS

After a comparison between the Boundary Perturbation Method and the Integral Equation Method for rough surface scattering computations we have used the Boundary Perturbation Method to produce and provide a software package for ocean surface scattering and ocean surface emissivity calculations. The first package is used in rain retrieval algorithms from PR using a "surface reference technique". The second package is used by EuroTRMM partners retrieving rain and atmospheric parameters from TMI. Finally, a synergic inversion of TRMM TMI and PR data was performed but with rather poor results.

References

F.L Bliven, P. Sobieski, C. Craeye, "Rain generated ring-waves : measurements and modelling for remote sensing", *Int. J. of Remote Sensing*, **18**, Nr 1,. 221-228, 1997.

M.L. Burrows, A reformulated boundary perturbation theory in electromagnetism and its application to a sphere, *Can. Jl. Phys.*,. **45**, 1729-1743, 1967.

M.L. Burrows, On the composite model for rough surface scattering, *IEEE Trans. Ant. and Prop.*, **AP-21**, 241-243, 1973.

C. Craeye, Radar signature of the sea surface perturbed by rain, *Ph. D. Thesis, Faculté des Sciences Appliquées, Université Catholique de Louvain, Belgium*, 280 p, 1998.

A.K. Fung, "Microwave Scattering and Emission Models and their Application", Artech House, 1994.

D. Lemaire, P. Sobieski, A. Guissard, Full-range sea surface spectrum in nonfully developed state for scattering computations, *IEEE Trans. Geosc. Rem. Sens.*, **37**, 1038-1051, 1999.

E.C. Monahan and M. Lu, "Acoustically relevant bubble assemblages and their dependance on meteorological parameters", *IEEE J. Ocean Engineer*, **15**, 340-349, 1990.

P. Sobieski and C. Craeye, Improved rain radar algorithms, *Workpackage report to ESA Contract 10146/NL/GS-CCN1*, Université Catholique de Louvain, TELE, 1997.